Correspondence

Generalised Poisson 3-D Scatterer Distributions

Catherine Laporte, James J. Clark, and Tal Arbel

***Abstract*—This paper describes a simple, yet powerful ultrasound scatterer distribution model. The model extends a 1-D generalized Poisson process to multiple dimensions using a Hilbert curve. The model is intuitively tuned by spatial density and regularity parameters which reliably predict the first- and second-order statistics of varied synthetic imagery.**

I. Introduction

Synthetic ultrasound (US) imagery is a powerful tool for the development and validation of US image processing algorithms. Because simulation permits fine-grained control over the ground truth imaging and target parameters, it is a very useful complement to real test imagery. Typical US simulators, such as Field II [1], [2], take as input a list of spatial coordinates corresponding to the location of point scatterers along with their scattering strength. The user must specify these parameters to reflect the object to be "scanned." As with real imagery, the texture of the resulting image depends on the structure of the scanned object (i.e., the type of tissue), which can be characterized by, among many parameters, the strength of the scatterers, their density, and their spatial organization. In the context of artificial US imagery used for the validation of image processing algorithms, most studies have focused on the first 2 of these parameters [3], [4]. Models for the spatial organization of US scatterers in multidimensional images exist, but have been geared mostly toward the study of clustering phenomena observed in blood [5], [6] rather than toward the development of a general purpose validation platform for image processing algorithms.

This paper demonstrates the power and flexibility of a general method, first introduced in [7], for generating lists of multidimensional scatterer positions with variable strength, density, and spatial organization ranging from tightly clustered to nearly regular to mimic a broad range of tissue types. The method extends a previous 1-D scatterer distribution model [8], [9] by mapping its output to a multidimensional space filling curve. The mapping provides a fast means of generating multidimensional data for simulations, and the characteristics of the resulting images are predictable from the model parameters. The stability and flexibility of the model are demonstrated by comparing the first- and second-order statistics of synthetic images produced using the model with theoretical predictions from US physics.

The rest of this paper is organized as follows. Section II presents the chosen adaptation of the 1-D model of [8], [9] to multiple dimensions. Section III compares the proposed model to other point distribution models used in ultrasonics literature. Section IV describes the pool of synthetic US data that was generated using the chosen model in conjunction with the Field II US simulator. In Section V, these data sets are used to validate the model against theoretical predictions of US speckle statistics based on previous US imaging research.

II. *M*-D Generalized Poisson Model

Consider a Poisson point process with rate $1/\beta$. In 1-D, this process can be defined in terms of statistics on the amount of space d between 2 consecutive points. These statistics are exponentially distributed. The approach taken in [8], [9] is to generalize the Poisson process by making d Gamma distributed instead of exponentially distributed:

$$f(d) = \frac{d^{\,\alpha-1}\exp(-d/\beta)}{\Gamma(\alpha)\beta^{\,\alpha}}, \quad \alpha,\beta,d > 0. \tag{1}$$

This distribution can be reparameterized in terms of the mean and variance of d, $\overline{d} = \alpha\beta$ and $\sigma_d^{\,d} = \alpha\beta^{\,2} = \overline{d}^{\,2}/\alpha$. The parameter α may then be viewed as a regularity parameter which, for a given point density, controlled by $1/\overline{d}$, tunes the variance of point spacing [9]. For $\alpha = 1$, (1) reduces to the exponential density, and the points are randomly distributed in space. For $\alpha < 1$, the point spacing has high variance and the points group in clusters, whereas for $\alpha > 1$, the point spacing has low variance, yielding nearly periodically spaced points.

This point process is intrinsically one-dimensional. Sampling this model becomes difficult in 2 or more dimensions, except in the trivial case $\alpha = 1$. A simple heuristic to generate 2-D points with $\alpha \neq 1$ would be to sample points according to the 1-D model along several short segments mapped to a 2-D grid of arbitrary precision in a raster scan fashion. This mapping poorly reflects what is really desired, as it only preserves the spatial organization of the original 1-D points along one direction. The raster scan mapping is but one of many possible continuous mappings of a line onto a finite multidimensional space known as

Manuscript received August 29, 2008; accepted September 2, 2008. This work was supported by doctoral scholarships from the Natural Science and Engineering Research Council of Canada, McGill University, and the Desjardins Foundation. Computational resources were provided by CLUMEQ and RQCHP.

The authors are with the Centre for Intelligent Machines, McGill University, Montreal QC H3A 2A7, Canada (e-mail: cathy@cim.mcgill.ca; clark@cim.mcgill.ca; arbel@cim.mcgill.ca).

Digital Object Identifier TBC

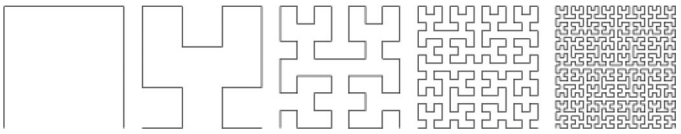

Fig. 1. Discrete approximations of the 2-D Hilbert curve [18]. The level of precision of the curves increases from 1 (left) to 5 (right).

space filling curves. More isotropic preservation of spatial organization can be achieved by using a different kind of space filling curve. Ideally, distances measured along the original line should correlate well with distances measured in the multidimensional space, a property known as preservation of locality. The Hilbert curve (shown in Fig. 1) is a recursively defined fractal curve which exhibits excellent preservation of locality and is therefore a good choice [10].

The algorithm introduced in [12] can be used to efficiently determine the mapping of 1-D points onto a m-dimensional Hilbert curve of a given precision. As a result of applying a Hilbert curve mapping to the output of the 1-D generalized Poisson point process, a set of m-D points is obtained whose spatial organization displays similar characteristics to that of the original 1-D points, as supported by empirical evidence of the preservation of local scatterer count statistics [7].

III. Comparison With Other Models

The power and flexibility of the proposed model are best demonstrated in comparison with alternative point process models. This section focuses on multidimensional models studied within the context of US scattering. In [5], the Neyman-Scott point process is used to generate clustered point patterns for the study of the characteristics of US signals in relation to red blood cell aggregation. Using this method, cluster centers are generated according to a Poisson process of a certain density. The actual data points are then generated according to the desired scatterer density from Gaussians centered about these cluster centers, whose variance σ^2 controls the tightness of the clusters. Sample 2-D point patterns obtained using this model are shown in Fig. 2(a), with the points taking a more tightly clustered configuration with larger σ. In these examples, the density of the cluster centers was taken to be the square root of the point density.

At the other end of the spatial organization continuum, quasi-regular point patterns can be generated by randomly jittering a lattice of regularly spaced points of a given density [13]. The randomness of the points is controlled by the variance κ^2 of a Gaussian noise process, as shown in Fig. 2(b).

Neither of these approaches models the full continuum of spatial organizations ranging from tightly clustered to nearly regular. Such flexibility is embodied in Gibbs-Markov pairwise interaction point processes, which describe stochastic repulsive and attractive potentials on pairs of

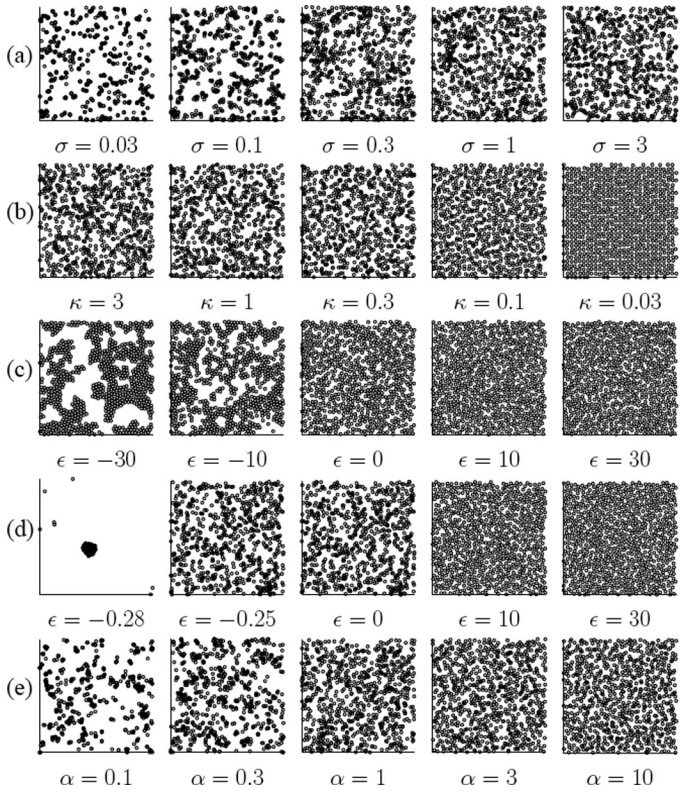

Fig. 2. Example 2-D point distributions obtained using different models with fixed point density. (a) Neyman-Scott process with varying cluster width σ; (b) Regular lattice with varying jitter noise κ; (c) Gibbs-Markov process with short-range repulsion and varying long-range potential ε; (d) Gibbs-Markov process with no short-range repulsion and varying long-range potential ε; (e) proposed generalized Poisson process with varying regularity parameter α.

points. Such a model was implemented in [6] to model aggregates of nonoverlapping red blood cells. A fixed, strong repulsive potential V enforced the latter constraint for pairwise distances below the diameter of a cell, while a distance dependent moderate potential ε drew points toward a clustered or regular (depending on the sign of the potential) configuration for a range of larger distances. Fig. 2(c) illustrates point configurations obtained using a very similar model. Note how, for clustered configurations, the strong short-range repulsive potential introduces regular structure within the clusters. This same short-range potential also prevents the formation of truly random point configurations. Fig. 2(d) shows what happens when the short-range potential is eliminated: for negative long-range potentials, the point configuration abruptly goes from random to extremely clustered, limiting the diversity of available clustered patterns [14]. As well as being difficult to tune, this sort of model is typically sampled using slow iterative algorithms whose convergence is difficult to assess.

Fig. 2(e) shows example 2-D point distributions obtained using the proposed model for a fixed point density and different values of α. Note how the point configurations smoothly transition from clustered, to random, to more regularly spaced with changes inα, making the model

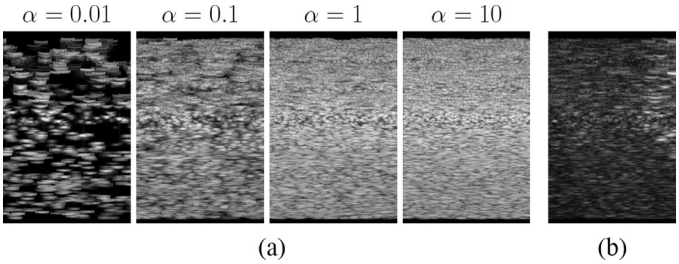

Fig. 3. Sample synthetic US images (a) obtained at 0.5 scatterer/mm^3 for different values of α; (b) obtained from a 3-D data set containing 10 different tissue types.

flexible and easy to tune. Table I summarizes the features of the different models compared in this section.

IV. Synthetic US Data Sets

The method described in Section II was used to generate lists of 3-D scatterer positions for all combinations of 6 scatterer density values ranging from 0.5 to 16 scatterers/mm^3 and 10 regularity parameter values ranging from 0.01 to 300, with logarithmic increments. The strength of each scatterer was chosen according to a lognormal distribution with mean 0.1 and variance 0.3 as suggested by [9]. Synthetic US data were generated from these lists of scatterers by Field II [1], [2] using a virtual linear array transducer with a central frequency of 3.5 MHz, a depth of 6 cm, a focus at 3 cm and a sampling frequency of 50 MHz. For each parameter setting, 100 parallel 2-D images were generated, separated by 0.1-mm increments and consisting of 128 radio-frequency (RF) vectors covering a width of 4 cm. The scatterers occupied a cubic volume of 6 $\times$ 6 $\times$ 6 cm, 2 mm below the transducer surface. The RF data were envelope detected using the Hilbert transform.

Slices from the 3-D data sets obtained for 0.5 scatterer/mm^3, logarithmically compressed for visualization, are shown in Fig. 3(a), illustrating how the image texture varies from a very grainy to a relatively smooth aspect as the regularity parameter increases. It is straightforward to combine different types of microstructure in the same data set to simulate a nonhomogeneous target. Fig. 3(b) shows one slice of a data set made from 10 different combinations of scatterer density, regularity, and strength distributions.

V. Speckle Statistics of Synthetic Imagery

To be useful in the context of US image simulation, the proposed scatterer distribution model must be able to produce a broad variety of speckle images. Additionally, the statistics of these images should be reliably predictable from the model parameters and agree with theory. This section examines the first- and second-order statistics of the synthetic imagery obtained using the proposed model.

A. First-Order Statistics

This section analyses 2 local first-order speckle statistics of the synthetic US data, namely the signal-to-noise ratio R and skewness S of the echo intensity signal I (the square of the envelope), defined as

$$R = \frac{E\{I\}}{\sqrt{\mathrm{VAR}\{I\}}} \text{ and } S = \frac{E\{(I - E\{I\})^3\}}{\mathrm{VAR}\{I\}^{3/2}}. \quad (2)$$

These quantities (or transformations thereof) parameterize many of the distributions commonly used to describe local speckle amplitude statistics, including the Rayleigh, K, Rician and homodyned K distributions [4] and the Nakagami distribution [16]. Theoretically, for Rayleigh scattering (high-density and randomly placed scatterers), R = 1 and S = 2. Lower density or tighter clustering of scatterers lead to lower values for R and higher values for S whereas the opposite may hold true when the scatterers are periodically placed along the direction of US wave propagation.

The synthetic data sets of Section IV were treated as collections of 100 2-D US image frames each. In each frame, 8 nonoverlapping windows measuring 14 A-lines laterally by 490 samples axially were studied at 4 different axial depths uniformly sampled within the image. Fig. 4 shows how R and S varies according to scatterer density, regularity, and axial depth.

As predicted by theory, as the scattering conditions approach those required for fully developed speckle formation, the value of R approaches 1 and S approaches 2. For a given depth and a random arrangement of the scatterers (α = 1), these results are obtained most closely for high scatterer densities. Clustering (low values of α) leads to so-called sub-Rayleigh conditions, with $R < 1$ and $S >$ 2, with low scatterer densities enhancing the effects of clustering. Also note the changes in R and S with depth,

TABLE I. Comparative Summary of Different Point Process Models Used in Ultrasonic Simulations.

Model	Params	Clusters	Regularity	Speed
Poisson	1	No	No	Very fast
Neyman-Scott	3	Yes	No	Very fast
Jittered lattice	2	No	Yes	Very fast
Gibbs-Markov	5	Yes	Yes	Slow
Generalized Poisson	2	Yes	Yes	Fast

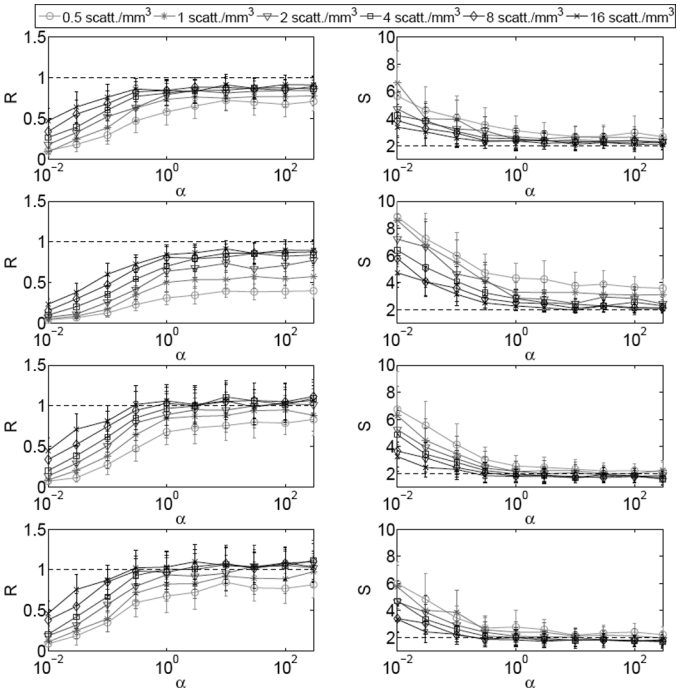

Fig. 4. Echo intensity first-order statistics as a function of scatterer density, regularity and axial depth. Left column: signal to noise ratio R. Right column: skewness S. Axial depth increases from top to bottom. The dashed lines mark the $R = 1$ and $S = 2$ lines representative of Rayleigh scattering conditions.

which are especially noticeable for low scatterer densities and small values of α. Near the focus (row 2), the local resolution cell size is at its smallest, thereby reducing the number of scatterers per resolution cell and leading to sub-Rayleigh conditions.

High values of α, corresponding to more regularly placed scatterers, do not appear to lead to conditions very different from Rayleigh scattering, with $R \approx 1$ and $S \approx 2$. This result is different from those presented in [9], where the original 1-D model with high regularity consistently led to positive interference patterns and Rician statistics ($R < 1$ and $S > 2$). The lack of systematic positive interference effects in the multidimensional model used here is due to the isotropy of the Hilbert curve mapping. While the model preserves regularity, there is absolutely no guarantee that this regularity will be aligned with a particular direction although, as shown by some of the 2-D results in [7], this *may* occur. For positive interference effects to invariably occur, the scatterers must be placed quasi-periodically in the direction of wave propagation, at multiples of the transmitted wavelength. Such patterns may be more systematically achieved through the choice of a different space filling curve to map the 1-D point process to 3-D. The Hilbert curve mapping nonetheless provides a useful and efficient multidimensional extension to the original 1-D point process on the basis of which a broad range of US image textures can be synthesized.

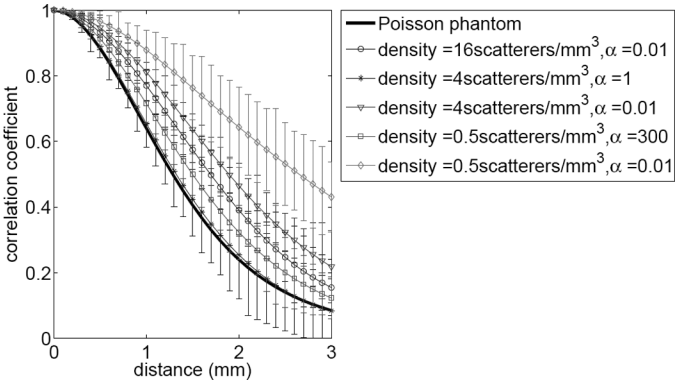

Fig. 5. Average elevational decorrelation curves at the transducer focus for a variety of combinations of scatterer density and regularity parameters.

B. Second-Order Statistics

Because of its finite beamwidth, an US transducer scanning the same target at 2 locations differing by a short distance images much of the same microstructure in both locations. The resulting images are therefore correlated, with the correlation decreasing monotonically with the distance between the 2 locations, a phenomenon known as speckle decorrelation. Under Rayleigh scattering conditions, the relationship between image correlation and the transducer's elevational displacement depends entirely on the transducer characteristics and can be described in a simple parametric form [17].

Fig. 5 shows the average correlation coefficient between pairs of image windows centered near the transducer focus as a function of their elevational separation for selected synthetic data sets. These are compared with the decorrelation curve for a data set obtained by placing scatterers at high density according to a plain Poisson process (without the Hilbert curve mapping), leading to Rayleigh scattering conditions. It was not difficult to find conditions for which the Rayleigh case decorrelation model fails to represent the behavior of the data, reflecting the results of [18] on imagery of real tissue. Also, note how the elevational second-order statistics of the synthetic data sets can be reliably predicted from the parameters of the proposed scatterer distribution model.

No principled parametric model exists which describes speckle decorrelation well in the general case. Such a model would be useful for applications like elevational transducer motion estimation based on speckle decorrelation [18]. A prospective application of the proposed scatterer distribution model would be to empirically establish a general speckle decorrelation model based on second-order statistics obtained from a large pool of synthetic imagery with known transducer motion and target structure.

VI. Conclusions

This paper presented a scatterer distribution model for which the density and spatial organization of scatterers can be tuned for the generation of varied synthetic US imagery. Spatial organization of the scatterers can be tuned along the continuum from clustered to regular in an intuitive manner, making the model attractive for the cross-tissue validation of US image processing algorithms through simulation studies. The synthetic platform allows fine-grained control over ground truth and target parameters which is at best difficult to achieve in phantom studies, thereby providing a useful complementary validation tool for image processing algorithms. This tool applies to a variety of contexts, a particularly relevant one being texture-based image segmentation.

In future work, different space filling curves can be studied for the generation of more or less anisotropic structures. Another area of interest is the study of the statistical properties of the synthetic imagery generated by the proposed model for the development of new image processing algorithms that adapt to local tissue structure.

References

[1] J. A. Jensen and N. B. Svendsen, "Calculation of pressure fields from arbitrarily shaped, apodized and excited ultrasound transducers," *IEEE Trans. Ultrason. Ferroelectr. Freq. Control*, vol. 39, no. 2, pp. 262–267, 1992.

[2] J. A. Jensen, "Field: A program for simulating ultrasound systems," in *Proc. Nordic-Baltic Conf. Biomedical Imaging*, vol. 4, 1996, pp. 351–353.

[3] J. A. Jensen and P. Munk, "Computer phantoms for simulating ultrasound B-mode and CFM images," in *Proc. 23rd Acoustical Imaging Symp.*, 1997, pp. 75–80.

[4] H. Liebgott, O. Bernard, C. Cachard, and D. Friboulet, "Field simulation parameters design for realistic statistical parameters of radiofrequency ultrasound images," in *Proc. IEEE Ultrasonics Symp.*, 2007, pp. 2247–2250.

[5] D. Savéry and G. Cloutier, "A point process approach to assess the frequency dependence of ultrasound backscattering by aggregating red blood cells," *J. Acoust. Soc. Am.*, vol. 110, no. 6, pp. 3252–3262, 2001.

[6] D. Savéry and G. Cloutier,, "Effect of red cell clustering and anisotropy on ultrasound blood backscatter: a Monte Carlo study," *IEEE Trans. Ultrason. Ferroelectr. Freq. Control*, vol. 52, no. 1, pp. 94–103, 2005.

[7] C. Laporte, J. J. Clark, and T. Arbel, "A fractal multidimensional ultrasound scatterer distribution model," in *Proc. IEEE ISBI*, 2007, pp. 880–883.

[8] L. Landini and L. Verrazzani, "Spectral characterization of tissues microstructure by ultrasounds: a stochastic approach," *IEEE Trans. Ultrason. Ferroelectr. Freq. Control*, vol. 37, no. 5, pp. 448–456, 1990.

[9] R. M. Cramblitt and K. J. Parker, "Generation of non-Rayleigh speckle distributions using marked regularity models," *IEEE Trans. Ultrason. Ferroelectr. Freq. Control*, vol. 46, no. 4, pp. 867–874, 1999.

[10] C. Gotsman and M. Lindenbaum, "On the metric properties of discrete space-filling curves," *IEEE Trans. Image Process.*, vol. 5, pp. 794–797, 1996.

[11] E. W. Weisstein. (1999) "Hilbert curve." *Mathworld – A Wolfram Web Resource.* Available: http://mathworld.wolfram.com/HilbertCurve.html.

[12] J. J. Bartholdi III and P. Goldsman, "Vertex-labeling algorithms for the Hilbert spacefilling curve," *Softw.: Pract. Exp.*, vol. 31, no. 5, pp. 395–408, 2000.

[13] V. M. Narayanan, R. C. Molthen, P. Shankar, L. Vergara, and J. Reid, "Studies on ultrasonic scattering from quasi-periodic structures," *IEEE Trans. Ultrason. Ferroelectr. Freq. Control*, vol. 44, no. 1, pp. 114–124, 1997.

[14] A. J. Baddeley and M. N. M. van Lieshout, "Area-interaction point processes," *Ann. Inst. Stat. Math.*, vol. 47, no. 4, pp. 601–619, 1995.

[15] V. Dutt and J. F. Greenleaf, "Ultrasound echo envelope analysis using a homodyned K distribution signal model," *Ultrason. Imaging*, vol. 16, no. 4, pp. 265–287, 1994.

[16] P. M. Shankar, "A general statistical model for ultrasonic backscattering from tissues," *IEEE Trans. Ultrason. Ferroelectr. Freq. Control*, vol. 47, no. 3, pp. 727–736, 2000.

[17] R. F. Wagner, S. W. Smith, J. M. Sandrik, and H. Lopez, "Statistics of speckle in ultrasound B-scans," *IEEE Trans. Sonics Ultrason.*, vol. 30, no. 3, pp. 156–163, 1983.

[18] A. H. Gee, R. J. Housden, P. Hassenpflug, G. M. Treece, and R. W. Prager, "Sensorless freehand 3D ultrasound in real tissue: speckle decorrelation without fully developped speckle," *Med. Image Anal.*, vol. 10, no. 2, pp. 137–149, 2006.